A New Vector Sensor Receiver for Underwater Acoustic Communication

Ali Abdi Huaihai Guo Patchara Sutthiwan

Center for Wireless Communication and Signal Processing Research
Electrical and Computer Engineering Department
New Jersey Institute of Technology
Newark, NJ, 07102, USA

Emails: ali.abdi@njit.edu, hg45@njit.edu, ps249@njit.edu

***Abstract*—In this paper we have shown that by taking advantage of the acoustic particle velocity, in addition to the acoustic pressure, multichannel reception can be accomplished in underwater channels. Theoretical formulation and Monte Carlo simulations are provided for a vector sensor equalizer that measures the pressure and the velocity at a single point in space. These results demonstrate the usefulness of a compact vector sensor as a multichannel equalizer.**

***Keywords*—Underwater communication, acoustic vector sensor, acoustic communication, multichannel equalization, acoustic particle velocity.**

I. Introduction

A vector sensor is capable of measuring important non-scalar components of the acoustic field such as the particle velocity, which cannot be obtained by a single scalar pressure sensor. In the past few decades, extensive research has been conducted on the theory and design of vector sensors (see, for example, [1]-[3]). They have been mainly used for underwater target localization and SONAR applications.

On the other hand, underwater acoustic communication systems have been relying on scalar sensors only, which measure the pressure of the acoustic field. The novel idea of this paper is to take advantage of the vector components of the acoustic field, such as the particle velocity, sensed by a vector sensor at the receiver, for detecting the transmitted data. The small size of such receivers is due to the fact that a vector sensor measures the scalar and vector components of the acoustic field in a single point in space, therefore can serve as a compact multichannel receiver. This is different from the existing multichannel underwater receivers [4]-[7], which are composed of spatially separated pressure-only sensors, which may result in large-size arrays.

The rest of this paper is organized as follows. An overview of different types of vector sensors and their current applications are provided in Section II. Basic system equations for the proposed vector sensor receiver are derived in Section III, whereas multichannel equalization using a vector sensor is formulated in Section IV. Sections V and VI include simulation set up and results, and concluding remarks are provided in Section VII.

II. An Overview of Vector Sensors

A. Current Applications of Vector Sensors

The development of vector sensors dates back to 30's [8]. Since late 60's, the Navy has been using vector sensors in systems such as Directional Frequency Analysis and Recording (DIFAR) and Directional Command Activated Sonobuoy System (DICASS) [9] [10]. In the past few decades, a large volume of research has been conducted on theory, performance evaluation, and design of vector sensors, mainly used in SONAR systems (see, for example, [1] and [2]). Examples include accurate azimuth and elevation estimation of a source [3] [11], avoiding the left-right ambiguity of linear towed arrays of scalar sensors, significant acoustic noise reduction due to the highly directive beam pattern [12] [13], etc. All these advantages are due to the directional information that vector sensors provide, by measuring the three orthogonal components of velocity, for example, as well as the pressure component, at a single point.

B. Different Types of Vector Sensors

In general, there are two types of vector sensors: inertial and gradient [14]. Inertial sensors truly measure the velocity or acceleration by responding to the acoustic particle motion, whereas gradient sensors employ a finite-difference approximation to estimate the gradients of the acoustic field such as velocity and acceleration. Each sensor type has its own advantages and disadvantages. Inertial sensors offer a broad dynamic range, but proper supporting and packaging of the sensor without affecting its response to the motion is an issue. Furthermore, since they do not distinguish between acoustic waves and non-acoustic motion sources such as support structure vibrations, they must be properly shielded from such disturbances. Making accurate yet small inertial sensors at high frequencies could be challenging as well. On the other hand, gradient sensors can be manufactured in smaller sizes and thus are more suitable for high frequencies. However, the finite-difference approximation which is the basis of operation of these sensors limits their operating dynamic range. Moreover, the individual elements of a gradient sensor are

required to have low self-noise and should be well calibrated and matched.

Recent progress in material science and manufacturing technologies for vector sensors is offering small size, low noise, and robust sensors (see [15] as an example). All these manufacturing advances certainly encourage the widespread use of vector sensors in many more underwater naval and civilian applications, including the vector sensor communication system proposed and developed in this paper. However, the proposed ideas, to take advantage of the vector components of the field at the receiver, are not restricted to a particular sensor type. Of course the noise properties, input dynamic range, bandwidth, sensitivity, and other characteristics of a vector sensor affect the reception performance, but the principles, models, and concepts developed in this paper remain nearly the same. Depending on the application, system cost, required precision, etc., one can choose the proper sensor type and technology.

III. System Equations in a Vector Sensor Receiver

In this section we derive basic system equations for data detection via a vector sensor. To demonstrate the basic concepts of how both the vector and scalar components of the acoustic field can be utilized for data reception, we consider a simple system in a two-dimensional (2D) depth-range underwater channel. As shown in Fig. 1, there is one transmit pressure sensor, shown by a black dot, whereas for reception we use a vector sensor, shown by a black square, which measures the pressure and the y and z components of the particle velocity. This is basically a 1×3 single-input multiple-output (SIMO) system. With more pressure transmitters, one can have a multiple-input multiple-output (MIMO) system, which is not included here due to space limitations.

A. Pressure and Velocity Channels and Noises

There are three channels in Fig. 1: the pressure channel p, represented by a straight dashed line, and two *pressure-equivalent* velocity channels p^z and p^y, shown by curved dashed lines. To define p^z and p^y, we need to define the two velocity channels v^z and v^y, the vertical and horizontal components of the particle velocity, respectively. According to the linearized momentum equation [12], the z and y component of the velocity at the frequency f_0 are given by

$$v^z = -(j\rho_0\omega_0)^{-1}\partial p/\partial z,\ v^y = -(j\rho_0\omega_0)^{-1}\partial p/\partial y\,. \qquad (1)$$

In the above equations, ρ_0 is the density of the fluid, $j^2=-1$ and $\omega_0 = 2\pi f_0$. Eq. (1) simply states that the velocity in a certain direction is proportional to the spatial pressure gradient in that direction [12]. To simplify the notation, similar to [12], the velocity channels in (1) are multiplied by $-\rho_0 c$, the negative of the acoustic impedance of the fluid, where c is the speed of sound. This gives the associated pressure-equivalent velocity channels as $p^z = -\rho_0 c\, v^z$ and $p^y = -\rho_0 c\, v^y$. With λ as the wavelength and $k = 2\pi/\lambda = \omega_0/c$ as the wavenumber, we finally obtain

$$p^z = (jk)^{-1}\partial p/\partial z,\ p^y = (jk)^{-1}\partial p/\partial y\,. \qquad (2)$$

The additive ambient noise pressure at the receiver is shown by n in Fig. 1. At the same location, the z and y components of the ambient noise velocity, sensed by the vector sensor, are $\eta^z = -(j\rho_0\omega_0)^{-1}\partial n/\partial z$ and $\eta^y = -(j\rho_0\omega_0)^{-1}\partial n/\partial y$, respectively, derived in the same manner as (1). So, the vertical and horizontal pressure-equivalent ambient noise velocities are $n^z = -\rho_0 c\,\eta^z = (jk)^{-1}\partial n/\partial z$ and $n^y = -\rho_0 c\,\eta^y = (jk)^{-1}\partial n/\partial y$, respectively, which resemble (2).

B. Input-Output System Equations

According to Fig. 1, the received pressure signal at *Rx* in response to the signal s transmitted from *Tx* can be written as $r = p \oplus s + n$, where $\oplus$ stands for convolution in time. We also define the z and y components of the pressure-equivalent received velocity signals as $r^z = (jk)^{-1}\partial r/\partial z$ and $r^y = (jk)^{-1}\partial r/\partial y$, respectively. Based on (2) and by taking the spatial gradient of r with respect to z and y we easily obtain the key system equations

$$r = p\oplus s + n,\ r^y = p^y \oplus s + n^y,\ r^z = p^z \oplus s + n^z\,. \qquad (3)$$

It is noteworthy that the three output signals r, r^y and r^z are measured at a single point in space.

C. Pressure and Velocity Noise Correlations

We define the spatial pressure noise correlation between the two locations $(y+\ell_y, z+\ell_z)$ and (y,z) as $q_n(\ell_y,\ell_z) = E[n(y+\ell_y, z+\ell_z)n^*(y,z)]$, where * is the complex conjugate and ℓ_y and ℓ_z are real numbers. Using the correlation properties of a differentiator in p. 326 of [16], at the location (y,z) one can show $E[n\{n^y\}^*] = (jk)^{-1}\partial q_n/\partial \ell_y$, $E[n\{n^z\}^*] = (jk)^{-1}\partial q_n/\partial \ell_z$ and $E[n^z\{n^y\}^*] = -k^{-2}\partial^2 q_n/\partial \ell_z \partial \ell_y$, all calculated for $(\ell_y,\ell_z)=(0,0)$. For an isotropic noise field in the y-z plane we have $q_n(\ell_y,\ell_z) = J_0(k(\ell_y^2+\ell_z^2)^{1/2})$ [17], with $J_m(.)$ as the m-order Bessel function of the first kind. Using the properties of the Bessel functions and their derivatives [18], it is easy to verify that $E[n\{n^y\}^*] = E[n\{n^z\}^*] = E[n^z\{n^y\}^*] = 0$, i.e., all the

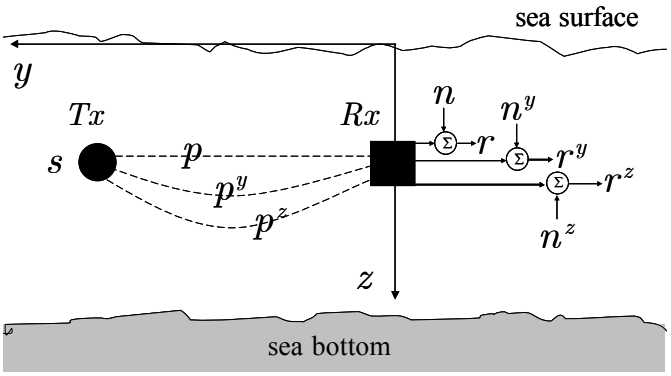

Fig. 1. A 1×3 vector sensor communication system, with one pressure transmitter and one vector sensor receiver. The vector sensor measures the pressure, as well as the y and z components of the acoustic particle velocity, all in a single point at the receive side. The system equations are given in (3).

noise terms in (3) are uncorrelated.

The above noise correlations may be derived using the general formulas of [19]. However, we have derived them from the first principles, to make it transparent to the readers under what conditions the noise terms in (3) are uncorrelated.

D. Pressure and Velocity Average Powers

1) Noise Powers: Using the statistical properties of a differentiator in p. 326 of [16], the powers of the y and z components of the pressure-equivalent noise velocity at (y,z) can be obtained as $\Omega_n^y = E[|\, n^y\,|^2] = -k^{-2}\partial^2 q_n / \partial \ell_y^2$ and $\Omega_n^z = E[|\, n^z\,|^2] = -k^{-2}\partial^2 q_n / \partial \ell_z^2$, respectively, both calculated at $(\ell_y, \ell_z) = (0,0)$. Based on the q_n of the 2D isotropic noise model described previously, one can show $\Omega_n^y = \Omega_n^z = 1/2$. Note that the noise pressure power in this model is $\Omega_n = E[|\, n\,|^2] = q_n(0,0) = 1$. This means $\Omega_n = \Omega_n^y + \Omega_n^z$, consistent with [19].

2) Channel Powers: The ambient noise is a superposition of several components coming from different angle of arrivals (AOAs) [17]. In multipath environments such as shallow waters, the channel is also a superposition of multiple subchannels. Based on this analogy between n and p, as well as their spatial gradients, one can obtain $\Omega_p = \Omega_p^y + \Omega_p^z$, where $\Omega_p = E[|\, p\,|^2]$, $\Omega_p^y = E[|\, p^y\,|^2]$ and $\Omega_p^z = E[|\, p^z\,|^2]$. The rigorous proof is not provided due to space limitations. In the 2D isotropic noise model the distribution of AOA is uniform over $[0, 2\pi)$ [17], which yields $\Omega_n^y = \Omega_n^z = \Omega_n / 2$. However, this is not necessarily the case in multipath channels such as shallow waters, which means Ω_p^y and Ω_p^z could be different.

E. Signal-to-Noise Ratios

To define the average signal-to-noise ratio (SNR) per channel in BER plots of Section VI, let $\mathbf{p} = [p(0) \ldots p(M-1)]^T$, $\mathbf{p}^y = [p^y(0) \ldots p^y(M-1)]^T$ and $\mathbf{p}^z = [p^z(0) \ldots p^z(M-1)]^T$ be the taps of the pressure, y- and z-velocity IRs, respectively. Then the pressure, y- and z-velocity SNRs are $\zeta_p = \Omega_p / \Omega_n$, $\zeta_p^y = \Omega_p^y / \Omega_n^y$ and $\zeta_p^z = \Omega_p^z / \Omega_n^z$, respectively, such that $\Omega_p = \mathbf{p}^\dagger \mathbf{p}$, $\Omega_p^y = (\mathbf{p}^y)^\dagger \mathbf{p}^y$ and $\Omega_p^z = (\mathbf{p}^z)^\dagger \mathbf{p}^z$. By definition, the average SNR per channel for the vector sensor receiver is $\overline{\zeta} = (\zeta_p + \zeta_p^y + \zeta_p^z)/3$. Also $\mathbf{p}$ is normalized such that $\Omega_p = 1$. Based on Subsection III.D, this implies that $\Omega_p^y + \Omega_p^z = 1$ in our simulations. Since $\Omega_n^y = \Omega_n^z = \Omega_n / 2$ in a 2D isotropic noise model, we finally obtain $\overline{\zeta} = 1/\Omega_n$, which is the same as the SNR of a unit-power pressure channel ζ_p.

IV. Vector Sensor as a Multichannel Equalizer

In this section we use the basic zero forcing equalizer. Of course there are different types of equalizers [20] [21] and we are not suggesting the zero forcing algorithm as the best possible equalization method. However, since here our emphasis is not on equalizer design, we just use a simple equalizer to verify the concept. The idea is just to demonstrate the feasibility of multichannel intersymbol-interference (ISI) removal using a compact vector sensor. Here the system equation is

$$\mathbf{R} = \mathbf{H}\mathbf{S} + \mathbf{N}, \text{ where } \mathbf{R} = \begin{bmatrix} \mathbf{R}_1 \\ \mathbf{R}_2 \\ \mathbf{R}_3 \end{bmatrix}, \mathbf{H} = \begin{bmatrix} \mathbf{H}_1 \\ \mathbf{H}_2 \\ \mathbf{H}_3 \end{bmatrix}, \text{ and } \mathbf{N} = \begin{bmatrix} \mathbf{N}_1 \\ \mathbf{N}_2 \\ \mathbf{N}_3 \end{bmatrix}. \quad (4)$$

In (4) $\mathbf{S} = [s_0 \ldots s_{K-1}]^T$ includes K transmitted symbols and ^{T} is the transpose. With M as the number of channel taps, the same for all l, $l = 1, 2, 3$, $\mathbf{R}_l = [r_l(0) \ldots r_l(K+M-2)]^T$ and $\mathbf{N}_l = [n_l(0) \ldots n_l(K+M-2)]^T$ are the l-th $(K+M-1)\times 1$ received signal and noise vectors, respectively. Also the l-th $(K+M-1)\times K$ banded channel matrix is given by

$$\mathbf{H}_l = \begin{bmatrix} h_l(0) & & \\ \vdots & \ddots & h_l(0) \\ h_l(M-1) & \ddots & \vdots \\ & & h_l(M-1) \end{bmatrix}. \quad (5)$$

Note that for a vector sensor receiver, the channel indices 1, 2 and 3 in (4) represent the pressure, pressure-equivalent horizontal velocity and pressure-equivalent vertical velocity, respectively. So, based on (3), for an arbitrary discrete time index t we have $r_1(t) = r(t)$, $r_2(t) = r^y(t)$, $r_3(t) = r^z(t)$, $h_1(t) = p(t)$, $h_2(t) = p^y(t)$, $h_3(t) = p^z(t)$, $n_1(t) = n(t)$, $n_2(t) = n^y(t)$ and $n_3(t) = n^z(t)$. Assuming perfect channel knowledge at the receiver, the zero forcing equalizer is

$$\hat{\mathbf{S}} = (\mathbf{H}^\dagger \mathbf{H})^{-1}\, \mathbf{H}^\dagger \mathbf{R}, \quad (6)$$

with $\hat{\mathbf{S}}$ as the estimate of $\mathbf{S}$ and † as the transpose conjugate. The simulations of Section VI show the performance of (6).

Since it is difficult to obtain perfect channel estimates at the receiver, in this paper we also study the impact of imperfect channel estimate on the vector sensor equalizer performance. We model the effect of channel estimation error using an additive Gaussian perturbation term

$$\begin{aligned} \hat{\mathbf{p}} &= \sqrt{\zeta_p/(1+\zeta_p)}\,\mathbf{p} + \sqrt{1/(1+\zeta_p)}\,\mathbf{e}, \\ \hat{\mathbf{p}}^y &= \sqrt{\zeta_p^y/(1+\zeta_p^y)}\,\mathbf{p}^y + \sqrt{1/(1+\zeta_p^y)}\,\mathbf{e}^y, \\ \hat{\mathbf{p}}^z &= \sqrt{\zeta_p^z/(1+\zeta_p^z)}\,\mathbf{p}^z + \sqrt{1/(1+\zeta_p^z)}\,\mathbf{e}^z, \end{aligned} \quad (7)$$

where $\hat{\mathbf{p}}$, $\hat{\mathbf{p}}^y$, and $\hat{\mathbf{p}}^z$ are imperfect estimates of $\mathbf{p}$, $\mathbf{p}^y$, and $\mathbf{p}^z$, respectively. Moreover, $\mathbf{e}$, $\mathbf{e}^y$, and $\mathbf{e}^z$ are $M\times 1$ Gaussian random vectors that represent channel estimation errors. Note that for each equation in (7), when the corresponding SNR is small, i.e., ζ_p, ζ_p^y or ζ_p^z, the estimation error term becomes dominant, as expected. On the other hand, when SNRs are large, we reasonably get $\hat{\mathbf{p}} \approx \mathbf{p}$, $\hat{\mathbf{p}}^y \approx \mathbf{p}^y$, and $\hat{\mathbf{p}}^z \approx \mathbf{p}^z$.

The vectors $\mathbf{e}$, $\mathbf{e}^y$, and $\mathbf{e}^z$ are independent, and elements of each vector are independent and identically distributed zero-mean complex Gaussian random variables with standard deviations $\sigma_p = \sqrt{\Omega_p / M}$, $\sigma_p^y = \sqrt{\Omega_p^y / M}$, and $\sigma_p^z = \sqrt{\Omega_p^z / M}$, respectively. Note that these choices for the standard deviations guarantee that the powers of the true channel coefficient vectors and their estimates are the same, i.e., $\hat{\Omega}_p = E[\hat{\mathbf{p}}^\dagger \hat{\mathbf{p}}] = \Omega_p$, $\hat{\Omega}_p^y = E[(\hat{\mathbf{p}}^y)^\dagger \hat{\mathbf{p}}^y] = \Omega_p^y$ and $\hat{\Omega}_p^z = E[(\hat{\mathbf{p}}^z)^\dagger \hat{\mathbf{p}}^z] = \Omega_p^z$.

In the presence of channel estimation error, the zero forcing

equalizer can be written as

$$\hat{\mathbf{S}}_{\text{ChEstErr}} = (\hat{\mathbf{H}}^{\dagger}\hat{\mathbf{H}})^{-1}\ \hat{\mathbf{H}}^{\dagger}\mathbf{R}\,, \tag{8}$$

where $\hat{\mathbf{S}}_{\text{ChEstErr}}$ is the estimate of $\mathbf{S}$, when $\mathbf{H}$ is not perfectly estimated, and $\hat{\mathbf{H}} = [\hat{\mathbf{H}}_1^T\ \hat{\mathbf{H}}_2^T\ \hat{\mathbf{H}}_3^T]^T$. Performance of (6) and (8) are also compared in Section VI via simulation.

V. Simulation Set up and Parameters

In this paper we basically simulate and compare the performance of the vector sensor equalizer in (6) and (8) with a vertical three-element pressure-only uniform linear array (ULA), as well as a single pressure sensor receiver that perform zero forcing equalization (with and without perfect channel estimate).

The ULA equations and equalizers are the same as (4), (6) and (8), where the three channels represent three vertically separated pressure channels. The noise vectors $\mathbf{N}_1, \mathbf{N}_2$ and $\mathbf{N}_3$ in both receivers are considered to be complex Gaussians with white temporal auto- and cross-correlations. For the isotropic noise model discussed in Subsection III.C, the noise vectors $\mathbf{N}_1, \mathbf{N}_2$ and $\mathbf{N}_3$ are uncorrelated in the vector sensor receiver. For the pressure-only ULA with the element spacing of λ, there are some small pressure correlations of $J_0(k\lambda) = 0.22$ and $J_0(2k\lambda) = 0.15$ for the separations of λ and 2λ, respectively, that are not included in the simulations.

With an $\mathbf{S}$ vector that includes $K = 200$ equal-probable ± 1 symbols, and the noise vector and channel matrix $\mathbf{N}$ and $\mathbf{H}$ generated as described above, the received vector $\mathbf{R}$ is calculated using (4). Then $\mathbf{S}$ is estimated using (6) and (8), and the bit error rate (BER) curves are plotted, as shown in Section VI. The parameters chosen to generate channel IRs are the same as [23] and are listed in Table I. Other receiver depths are considered in [24]. The sound speed profile we used was measured during the underwater communication experiments conducted on May 10, 2002, in waters off San Diego, CA [23], and is shown in Fig. 2.

VI. Simulation Results and Performance Comparison

According to Table I, there are four propagation scenarios
- Scenario 1: 5 km range and coarse silt bottom,
- Scenario 2: 10 km range and coarse silt bottom,
- Scenario 3: 5 km range and very fine sand bottom,
- Scenario 4: 10 km range and very fine sand bottom.

In the following subsections first we show channel impulse responses and frequency responses for these four scenarios. Then we study the delay spread and the horizontal to vertical velocity power ratio versus range and depth, for different bottom types. Afterwards, we present BER and eigenvalue curves for the above four scenarios, which demonstrate the performance of the proposed vector sensor receiver, as well as a pressure-only array receiver and a single pressure sensor receiver. At the end the impact of channel estimation error is discussed.

TABLE I
SIMULATION AND CHANNEL PARAMETERS

Water Depth (m)	81.158
Water Density (kg/m^3)	1024
Transmitter Depth (m)	25
Transmit Take-off Angle (degree)	-30 to 30
Number of Beams	2001
Bottom Types	Coarse silt, Very fine sand
Receiver Depth (m)	63
Receiver Range (km)	5, 10
Carrier Frequency (kHz)	12
Sampling Frequency (kHz)	48
Data Rate (kbps)	2.4
Nominal Sound Speed (m/s)	1500
Wavelength (m)	0.125

A. Impulse Response and Frequency Response

The amplitudes of the complex impulse responses of the above four propagation scenarios are shown in Figs. 3a, 4a, 5a and 6a. Each figure includes the impulse responses of the pressure, horizontal velocity and vertical velocity channels, with powers Ω_p, Ω_p^y and Ω_p^z defined in Subsection III.E, respectively. To obtain the velocity channel impulse responses p^y and p^z from the p channel impulse response generated by Bellhop [22], each spatial gradient in (2) is approximated by a finite difference. Therefore at location (y,z) we have $\partial p(y,z)/\partial z \approx [p(y,z+0.2\lambda) - p(y,z)]/(0.2\lambda)$ and $\partial p(y,z)/\partial y \approx [p(y+0.2\lambda,z) - p(y,z)]/(0.2\lambda)$. The number of channel taps and the powers of horizontal and vertical velocity channels in the simulations are given below
- Scenario 1: $M = 147$, $\Omega_p^y = 0.42$, $\Omega_p^z = 0.58$,
- Scenario 2: $M = 197$, $\Omega_p^y = 0$, $\Omega_p^z = 1$,
- Scenario 3: $M = 460$, $\Omega_p^y = 0.39$, $\Omega_p^z = 0.61$,
- Scenario 4: $M = 846$, $\Omega_p^y = 0.03$, $\Omega_p^z = 0.97$.

Notice that in Scenarios 2 and 4, the power of the horizontal velocity channel is much smaller than the vertical velocity channel. This issue will be further investigated later in the paper. As mentioned in Subsection III.E, the pressure channel in simulations is normalized to have unit power, i.e., $\Omega_p = 1$, and

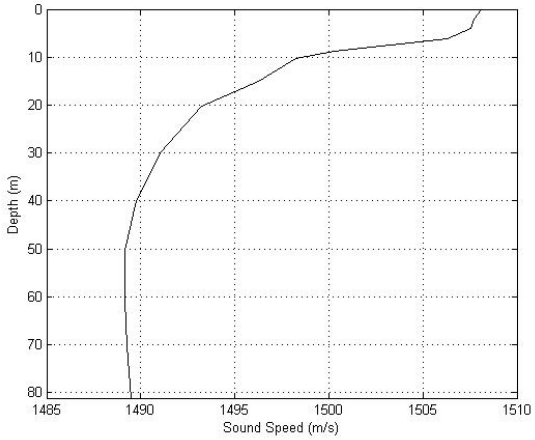

Fig. 2. Sound speed versus the water depth.

also $\Omega_p^y + \Omega_p^z = 1$.

The amplitudes of the Fourier transforms of the impulse responses of Figs. 3a, 4a, 5a and 6a are shown in Figs. 3b, 4b, 5b and 6b, respectively. Each figure includes the frequency responses of the pressure, horizontal velocity and vertical velocity channels.

B. Delay Spread

In this subsection we look at the root-mean-squared (RMS) delay spread τ_{rms} [25] as a measure of the frequency selectivity of a channel. Typically a large delay spread indicates a highly frequency selective channel. The values of τ_{rms} for the four scenarios are given in Table II.

In Fig. 7, τ_{rms} of p, p^y and p^z impulse responses are plotted versus range, at 20, 40, and 60 m depths, for the coarse silt bottom. Then by averaging over these three depths, an average curve versus range is obtained for each of the p, p^y and p^z channels, as shown in Fig. 8 for the coarse silt bottom. Figs. 9 and 10 are similarly generated for the very fine sand bottom.

According to Figs. 7 and 9, delay spread of the p channel do not noticeably change with depth, compared to the delay spreads of p^y and p^z channels. Also based on Fig. 10, the very fine sand bottom, the depth-averaged delay spreads of p and p^z channels are almost the same. However, for the coarse silt bottom in Fig. 8, one can see more variations among the depth-averaged delay spreads of all the channels.

C. Horizontal to Vertical Velocity Power Ratio

The ratio Ω_p^y / Ω_p^z is plotted versus the receiver range in Figs. 11 and 12, for coarse silt and very fine sand bottoms, respectively. For each bottom type, first Ω_p^y / Ω_p^z is presented at three different depths which are 20, 40 and 60 m. Then by averaging over these three depths, a single average curve versus range is obtained for each bottom. According to Fig. 12, for the very fine sand bottom we have $\Omega_p^y / \Omega_p^z < 1$, for ranges up to 14 km. For the coarse silt bottom, however, Ω_p^y / Ω_p^z can take large values at certain depths and ranges, as shown in Fig. 11.

D. Bit Error Rate

The BER curves versus the average SNR per channel $\bar{\zeta}$, defined in Subsection III.E, are shown in Figs. 3c, 4c, 5c and 6c, for Scenarios 1-4, respectively. Each figure includes the BERs of a vector sensor receiver, a three-element pressure-only array receiver with element spacing λ and a single pressure sensor receiver. As expected, the performance of the single pressure sensor receiver is much worse than the other two receivers. The performance of the vector sensor receiver is slightly better than the pressure-only array. According to the summary of SNRs provided in Table III, the difference in performance ranges from 0.3 dB to 2.4 dB, among all the four scenarios. By changing the simulation scenario, for example the bottom type, frequency of operation, or inclusion of the flow noise and non-acoustic disturbances which are particularly important for inertial (motion) vector sensors, one may observe a worse performance for the vector sensor equalizer, compared to the pressure-only array equalizer. However, it is anticipated that the vector sensor and pressure-only array equalizers still will provide comparable performance, much superior to a single pressure sensor.

TABLE II
RMS DELAY SPREADS (msec.) IN FOUR PROPAGATION SCENARIOS

	Pressure channel	Horizontal velocity channel	Vertical velocity channel
Scenario 1	7.7	0.26	6.8
Scenario 2	14.8	12.9	11.4
Scenario 3	48.1	0.28	44.1
Scenario 4	90.3	4.3	68.3

One simple way of explaining the performance of these three zero forcing equalizers is to look at the condition number of $\mathbf{H}^\dagger\mathbf{H}$ in (6). By definition, the condition number of a matrix is the ratio of its largest singular value to the smallest one, and a large condition number implies that the matrix is nearly singular. This corresponds to more noise enhancement in the zero forcing equalizer, due to the inverse of $\mathbf{H}^\dagger\mathbf{H}$. Based on the condition numbers provided in Table III, calculated in Matlab®, one can see a better equalizer typically has a smaller condition number, as expected. For Scenario 3, however, vector sensor has a better performance in terms of BER, but with the higher condition number. To clarify this, one needs to look at the entire spectrum of the eigenvalues.

In Figs. 3d, 4d, 5d and 6d, the eigenvalues of $\mathbf{H}^\dagger\mathbf{H}$ are plotted for all the propagation scenarios and receivers, normalized such that the largest eigenvalue for each scenario and receiver is 1. As one can see, the eigenvalues of the vector sensor receiver are larger than those of other receivers. In Scenario 3, however, there are few small eigenvalues, nearly the same as other small eigenvalues. This is one possible explanation for the similar BER performance of the vector sensor and pressure-only array equalizers in Scenario 3.

E. Effect of Imperfect Channel Estimates

TABLE III
A SUMMARY OF THE REQUIRED SNRS FOR SPECIFIC BERS

	Equalizer	Cond. no.	SNR per chann. (dB)	
			BER=10^{-3}	BER=10^{-2}
Scen. 1	**Vector sensor**	**99**	**4.6**	**2.1**
	Pressure-only array	126	7	4.3
	Single pressure sensor	174	14	9.7
Scen. 2	**Vector sensor**	**16**	**5.2**	**2.7**
	Pressure-only array	292	6.7	4.2
	Single pressure sensor	297	9.2	6.8
Scen. 3	**Vector sensor**	**83**	**4.3**	**1.8**
	Pressure-only array	57	4.6	2.2
	Single pressure sensor	58	9.8	7.4
Scen. 4	**Vector sensor**	**12**	**2.5**	**0**
	Pressure-only array	23	4	1.4
	Single pressure sensor	25	8.6	6

In Fig. 13 we present the BERs for Scenario 1, with and without perfect channel estimates. As expected, equalization without exact knowledge of the channel matrix **H** results in a loss in SNR for all types of receivers. For example, at BER = 10^{-2}, the SNR loss for the vector sensor receiver is 3 dB.

VII. Summary and Conclusion

In this paper we have introduced and developed the concept of data detection and equalization in underwater communication channels using acoustic vector sensors. These sensors measure the acoustic pressure, as well as the components of the acoustic particle velocity. Basic system equations for such a receiver are derived and channel equalization using these sensors is formulated. Signal and noise power characteristics in such sensors are also investigated. Via extensive simulations under different propagation scenarios, the performance of a vector sensor equalizer is determined and compared with single and multiple pressure sensor receivers. The impact of channel estimation error on the receiver performance is also studied. The delay spreads of velocity channels are also investigated.

The overall message of the paper is that in the cases considered, the proposed vector sensor equalizer and the pressure-only array equalizer both outperform a single pressure sensor equalizer. The advantage of a vector sensor receiver is its smaller size, compared to pressure-only arrays.

The focus of this paper was mainly on the communication aspects of a vector sensor receiver. Those channel modeling and propagation issues of acoustic velocity channels that affect the system performance will be discussed in another paper.

Acknowledgement

We would like to thank Dr. Shuangquan Wang for useful discussions and comments.

References

[1] *Proc. AIP Conf. Acoustic Particle Velocity Sensors: Design, Performance, and Applications*, Mystic, CT, 1995.

[2] *Proc. Workshop Directional Acoustic Sensors (CD-ROM)*, New Port, RI, 2001.

[3] A. Nehorai and E. Paldi, "Acoustic vector-sensor array processing," *IEEE Trans. Signal Processing*, vol. 42, pp. 2481-2491, 1994.

[4] T. C. Yang, "Temporal resolutions of time-reversal and passive-phase conjugation for underwater acoustic communications," *IEEE J. Oceanic Eng.*, vol. 28, pp. 229–245, 2003.

[5] C. C. Tsimenidis, O. R. Hinton, A. E. Adams, and B. S. Sharif, "Underwater acoustic receiver employing direct-sequence spread spectrum and spatial diversity combining for shallow-water multi-access networking," *IEEE J. Oceanic Eng.*, vol. 26, pp. 594–603, 2001.

[6] D. Rouseff, D. R. Jackson, W. L. J. Fox, C. D. Jones, J. A. Ritcey, and D. R. Dowling, "Underwater acoustic communication by passive-phase conjugation: Theory and experimental results," *IEEE J. Oceanic Eng.*, vol. 26, pp. 821–831, Oct. 2001.

[7] M. Stojanovic, J. A. Catipovic, and J. G. Proakis, "Reduced-complexity spatial and temporal processing of underwater acoustic communication signals," *J. Acoust. Soc. Am.*, vol. 98, pp. 961–972, 1995.

[8] H. F. Olson, "Mass controlled electrodynamic microphones: the ribbon microphone," *J. Acoust. Soc. Am.*, vol. 3, pp. 56-68, 1931.

[9] M. E. Higgins, "DIFAR system overview," in *Proc. Workshop Directional Acoustic Sensors (CD-ROM)*, New Port, RI, 2001.

[10] M. T. Silvia and R. T. Richards, "A theoretical and experimental investigation of low-frequency acoustic vector sensors," in *Proc. Oceans*, Biloxi, MS, 2002, pp. 1886-1897.

[11] M. Hawkes and A. Nehorai, "Acoustic vector-sensor beamforming and Capon direction estimation," *IEEE Trans. Signal Processing*, vol. 46, pp. 2291-2304, 1998.

[12] B. A. Cray, V. M. Evora, and A. H. Nuttall, "Highly directional acoustic receivers," *J. Acoust. Soc. Am.*, vol. 113, pp. 1526-1532, 2003.

[13] B. A. Cray and A. H. Nuttall, "Directivity factors for linear arrays of velocity sensors," *J. Acoust. Soc. Am.*, vol. 110, pp. 324-331, 2001.

[14] T. B. Gabrielson, "Design problems and limitations in vector sensors," in *Proc. Workshop Directional Acoustic Sensors (CD-ROM)*, New Port, RI, 2001.

[15] J. Clay Shipps and K. Deng, "A miniature vector sensor for line array applications," in *Proc. Oceans*, San Diego, CA, 2003, pp. 2367-2370.

[16] A. Papoulis, *Probability, Random Variables, and Stochastic Processes*, 3rd ed., Singapore: McGraw-Hill, 1991.

[17] H. Cox, "Spatial correlation in arbitrary noise fields with application to ambient sea noise," *J. Acoust. Soc. Am.*, vol. 54, pp. 1289-1301, 1973.

[18] W. Magnus, F. Oberhettinger, and R. P. Soni, *Formulas and Theorems for the Special Functions of Mathematical Physics*, 3rd ed., New York: Springer, 1966.

[19] M. Hawkes and A. Nehorai, "Acoustic vector-sensor correlations in ambient noise," *IEEE J. Oceanic Eng.*, vol. 26, pp. 337-347, 2001.

[20] J. G. Proakis, *Digital Communications*, 4th ed., New York: McGraw-Hill, 2001.

[21] J. R. Barry, E. A. Lee and D. G. Messerschmitt, *Digital Communication*, 3rd ed., Boston, MA: Kluwer, 2004.

[22] Acoustics Toolbox http://www.cmst.curtin.edu.au/products/actoolbox/

[23] P. S. Duke, "Direct-sequence spread-spectrum modulation for utility packet transmission in underwater acoustic communication networks," M.S. thesis, Dept. Elec. Comp. Eng., Naval Postgraduate School, Monterey, CA, 2002.

[24] P. Sutthiwan, "Multichannel underwater communication receivers," M.S. project report, Dept. Elec. Comp. Eng., New Jersey Institute of Technology, Newark, NJ, 2006.

[25] T. S. Rappaport, *Wireless Communications: Principles and Practice*, 2nd ed., Upper Saddle River, NJ: Prentice Hall, 2002.

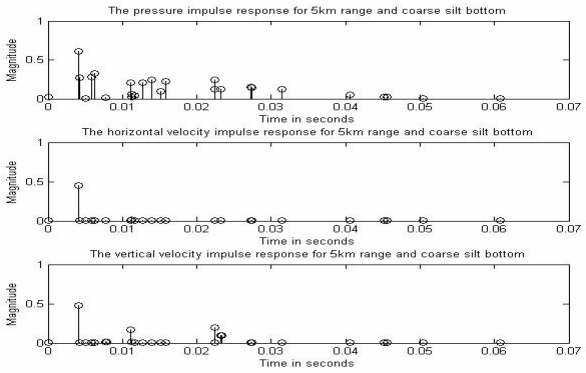

Fig. 3a. The amplitude of the impulse responses in Scenario 1.

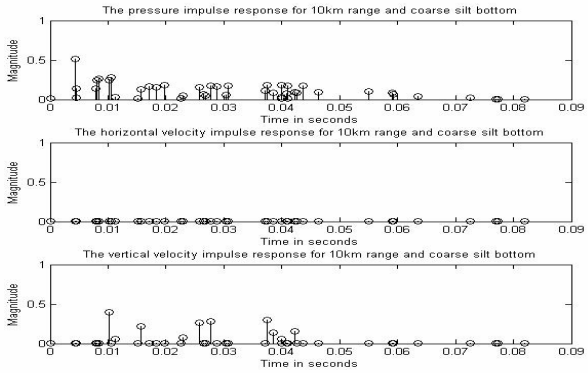

Fig. 4a. The amplitude of the impulse responses in Scenario 2.

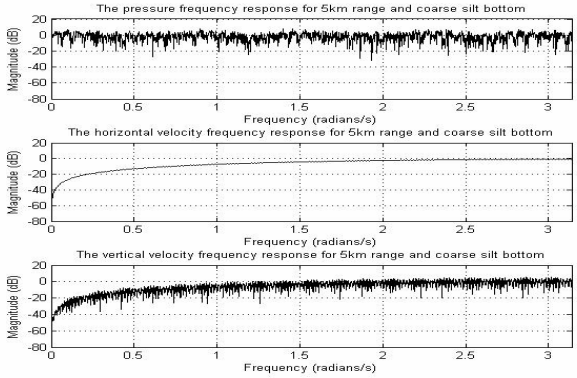

Fig. 3b. The amplitude of the frequency responses in Scenario 1.

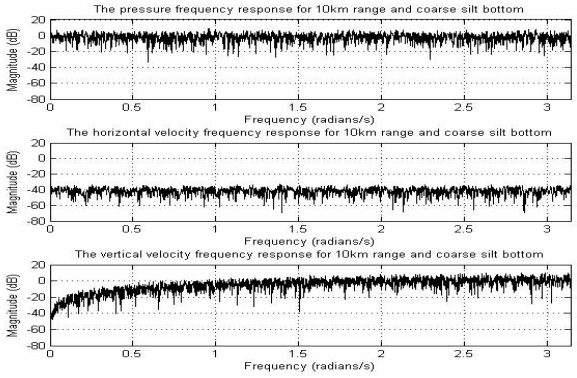

Fig. 4b. The amplitude of the frequency responses in Scenario 2.

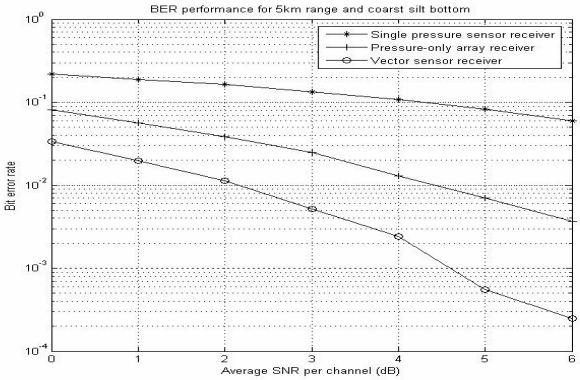

Fig. 3c. BER performance of equalizers in Scenario 1.

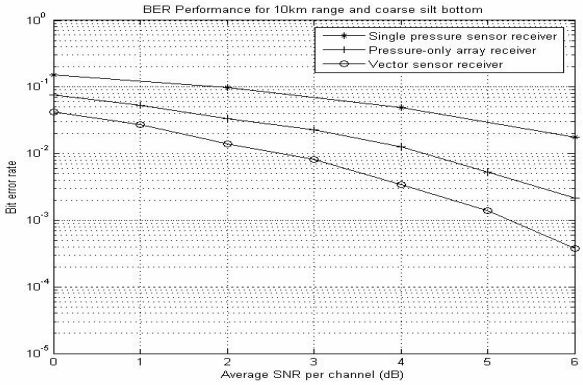

Fig. 4c. BER performance of equalizers in Scenario 2.

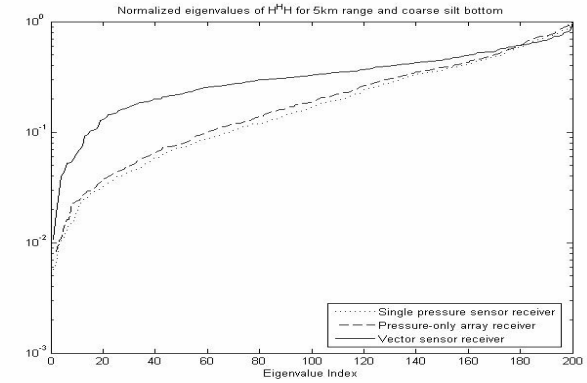

Fig. 3d. Normalized eigenvalues of $\mathbf{H}^{\dagger}\mathbf{H}$ in Scenario 1.

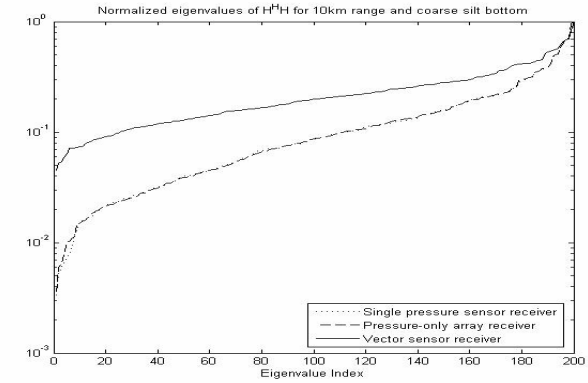

Fig. 4d. Normalized eigenvalues of $\mathbf{H}^{\dagger}\mathbf{H}$ in Scenario 2.

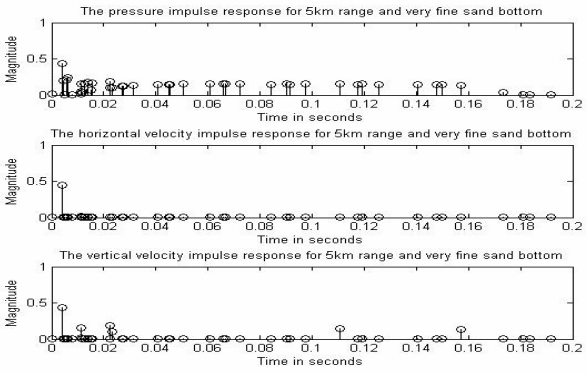

Fig. 5a. The amplitude of the impulse responses in Scenario 3.

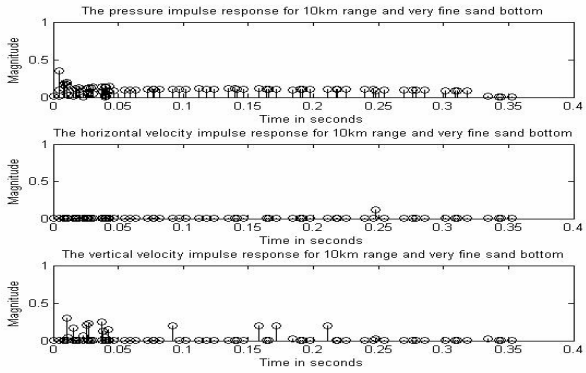

Fig. 6a. The amplitude of the impulse responses in Scenario 4.

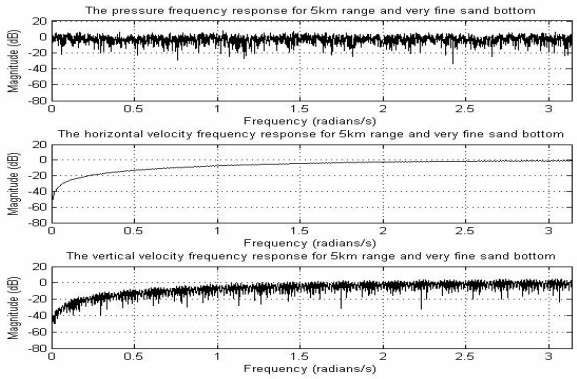

Fig. 5b. The amplitude of the frequency responses in Scenario 3.

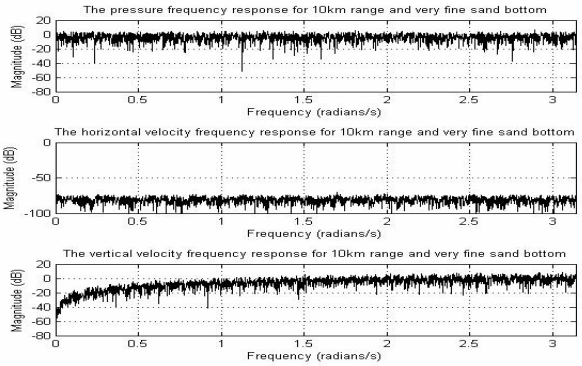

Fig. 6b. The amplitude of the frequency responses in Scenario 4.

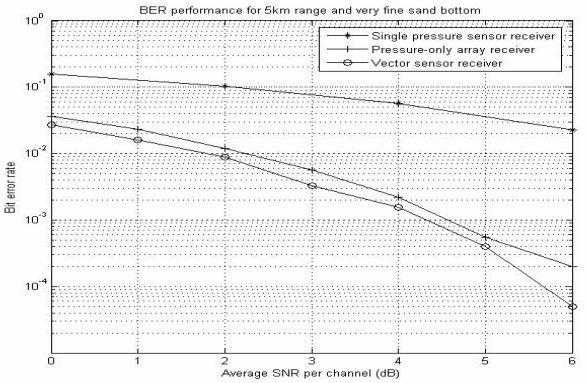

Fig. 5c. BER performance of equalizers in Scenario 3.

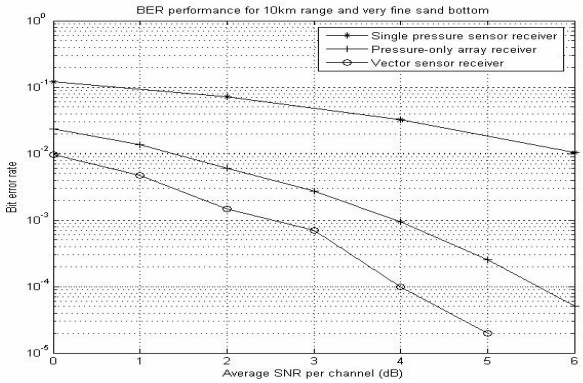

Fig. 6c. BER performance of equalizers in Scenario 4.

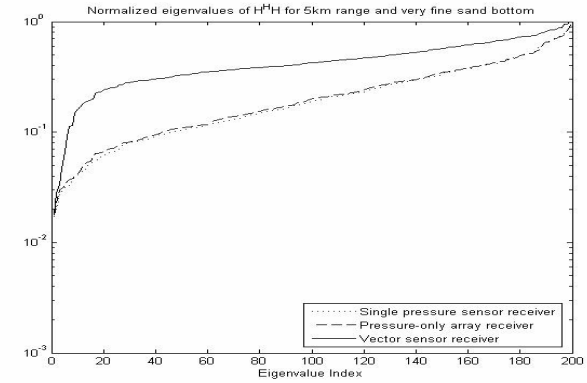

Fig. 5d. Normalized eigenvalues of $\mathbf{H}^{\dagger}\mathbf{H}$ in Scenario 3.

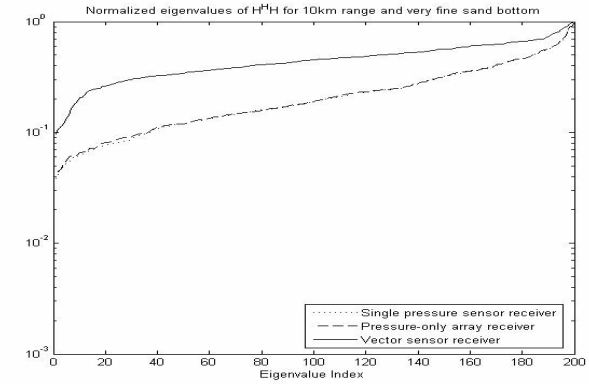

Fig. 6d. Normalized eigenvalues of $\mathbf{H}^{\dagger}\mathbf{H}$ in Scenario 4.

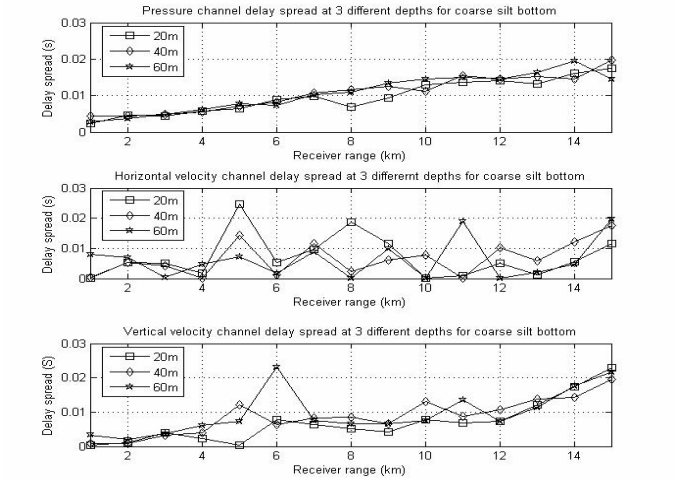

Fig. 7. Delay spread versus range for the coarse silt bottom at different depths. Top: pressure channel, Middle: horizontal velocity channel, Bottom: vertical velocity channel.

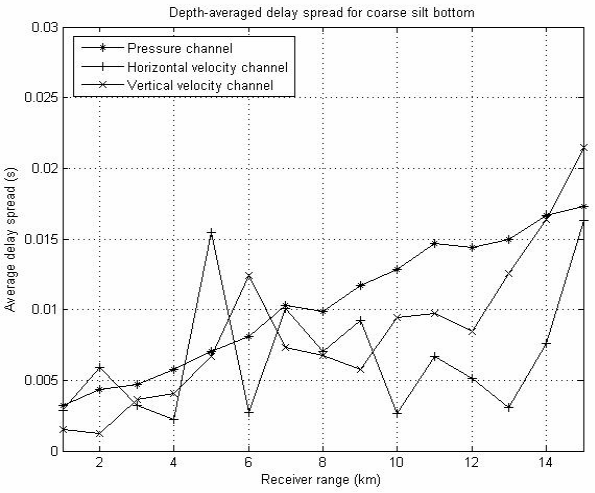

Fig. 8. Depth-averaged delay spread versus range for the coarse silt bottom.

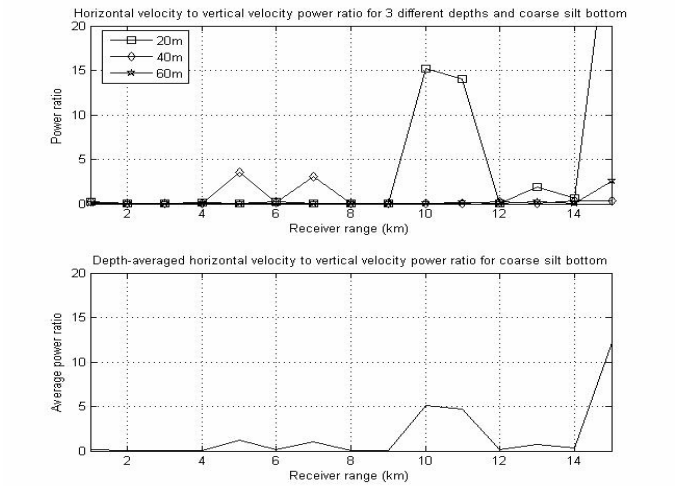

Fig. 11. Horizontal to vertical velocity power ratio versus range for the coarse silt bottom. Top: different depths, Bottom: averaged over different depths.

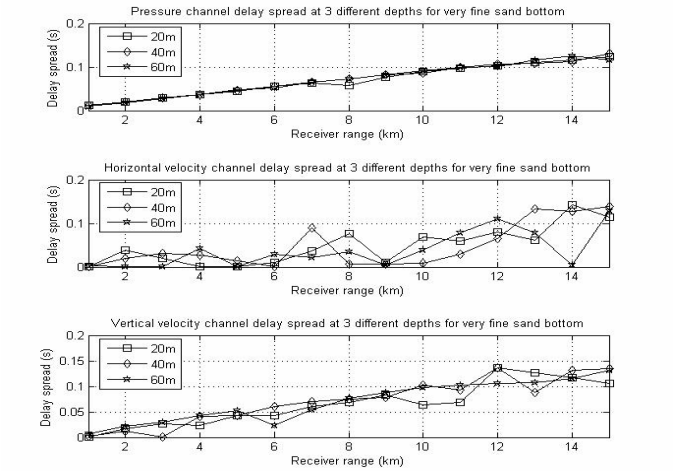

Fig. 9. Delay spread versus range for the very fine sand bottom at different depths. Top: pressure channel, Middle: horizontal velocity channel, Bottom: vertical velocity channel.

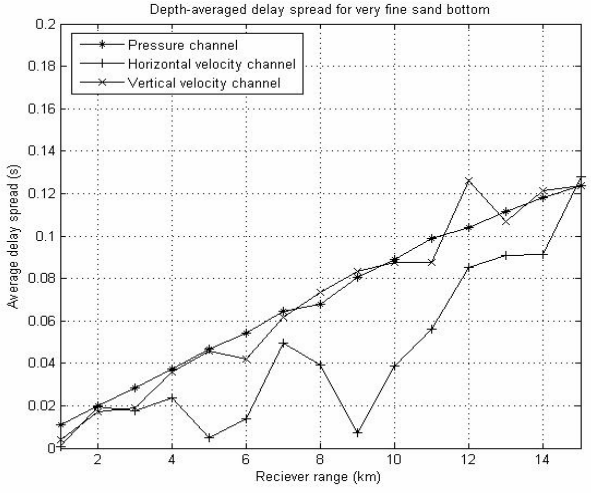

Fig. 10. Depth-averaged delay spread versus range for very fine sand bottom.

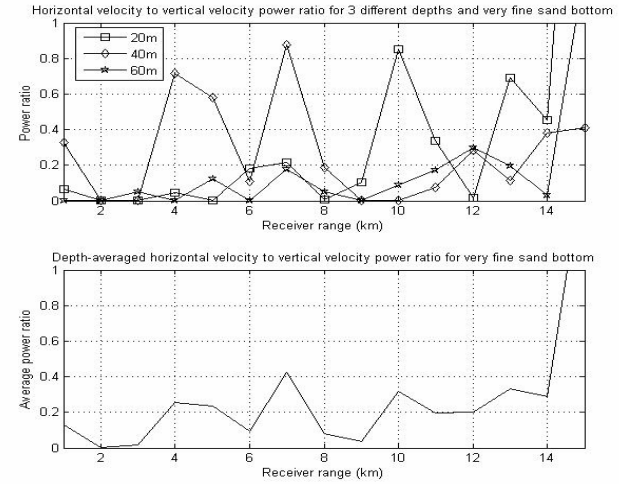

Fig. 12. Horizontal to vertical velocity power ratio versus range for the very fine sand bottom. Top: different depths, Bottom: averaged over different depths.

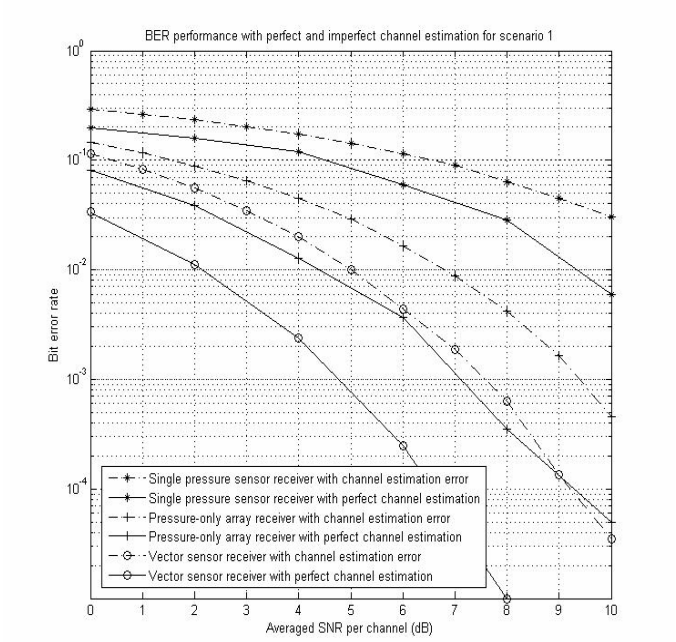

Fig. 13. The impact of imperfect channel estimate on the performance of vector sensor and pressure-only equalizers in Scenario 1.